Supplementary information

Supplementary Figures

Supplementary Figure 1

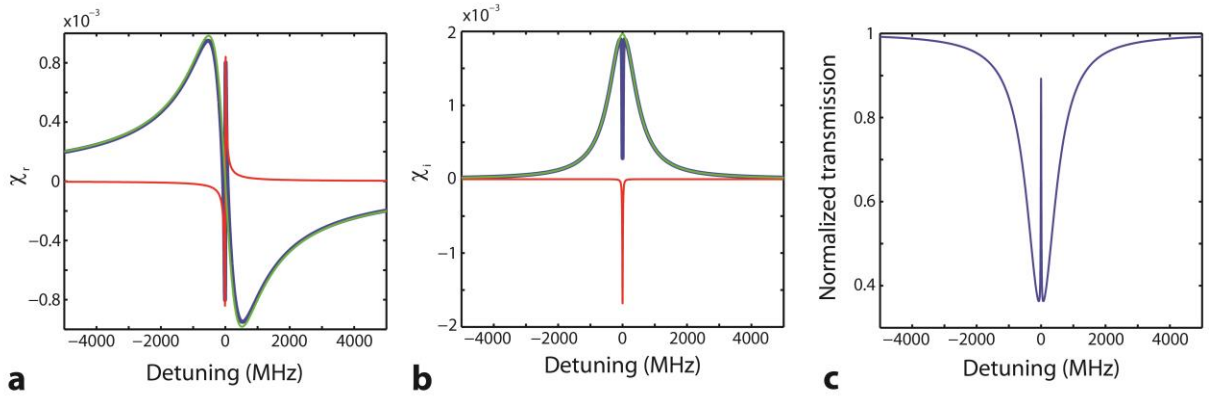

Supplementary Figure 1. Real and imaginary parts of the susceptibility χ in the weak driving regime. *(**a**) Real part of the susceptibility. (Blue: $\chi_{r1}+\chi_{r2}$, red: χ_{r1}, green: χ_{r2}). (**b**) Imaginary part of the susceptibility. (Blue: $\chi_{i1}+\chi_{i2}$, red: χ_{i1}, green: χ_{i2}). (**c**) Normalized transmission. The parameters used in (a)-(c) were obtained in the experiments: Decay rate of the first resonator was $\gamma_1 = 1.05\,\mathrm{GHz}$; decay rate of the second resonator was $\gamma_2 = 3\,\mathrm{MHz}$ and coupling strength was $\kappa = 67\,\mathrm{MHz}$.*

Supplementary Figure 2

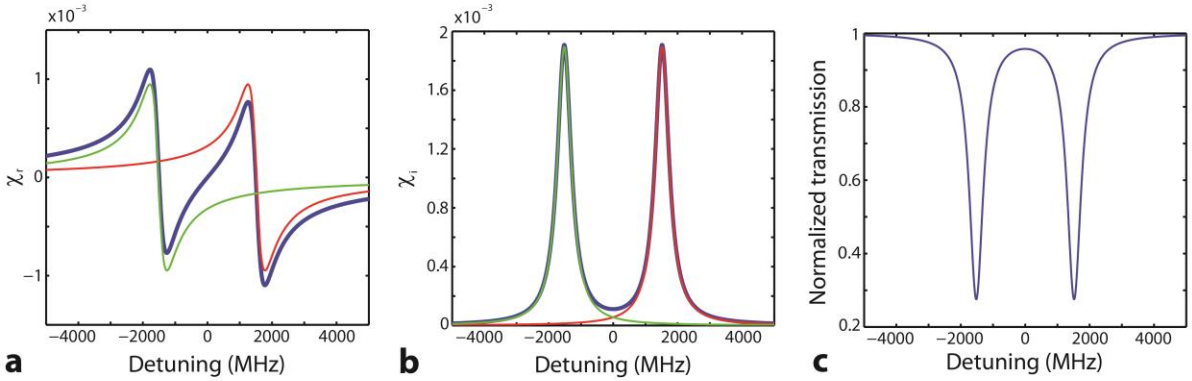

Supplementary Figure 2. Real and imaginary parts of the susceptibility χ in the strong driving regime. *(**a**) Real part of the susceptibility. (Blue: $\chi_{r1}+\chi_{r2}$, red: χ_{r1}, green: χ_{r2}). (**b**) Imaginary part of the susceptibility. (Blue: $\chi_{i1}+\chi_{i2}$, red: χ_{i1}, green: χ_{i2}). (**c**) Normalized transmission. The parameters used in (a)-(c) were obtained from experiments: Decay rate of the first resonator was $\gamma_1 = 1.05\,\mathrm{GHz}$; decay rate of the second resonator was $\gamma_2 = 3\,\mathrm{MHz}$; coupling strength was $\kappa = 1.52\,\mathrm{GHz}$*

Supplementary Figure 3

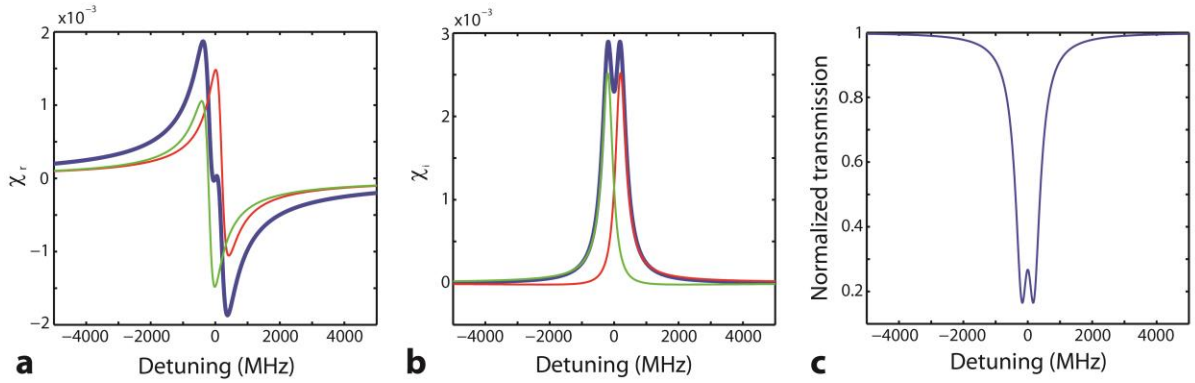

Supplementary Figure 3. Real and imaginary parts of the susceptibility χ in the intermediate-driving regime. ***(a)*** *Real part of the susceptibility. (Blue: $\chi_{r1}+\chi_{r2}$, red: χ_{r1}, green: χ_{r2}).* ***(b)*** *Imaginary part of the susceptibility. (Blue: $\chi_{i1}+\chi_{i2}$, red: χ_{i1}, green: χ_{i2}).* ***(c)*** *Normalized transmission. The parameters used were obtained from experiments. Decay rate of the first resonator was $\gamma_1 = 462\ \mathrm{MHz}$; decay rate of the second resonator was $\gamma_2 = 337\ \mathrm{MHz}$; coupling strength was $\kappa = 186\ \mathrm{MHz}$.*

Supplementary Figure 4

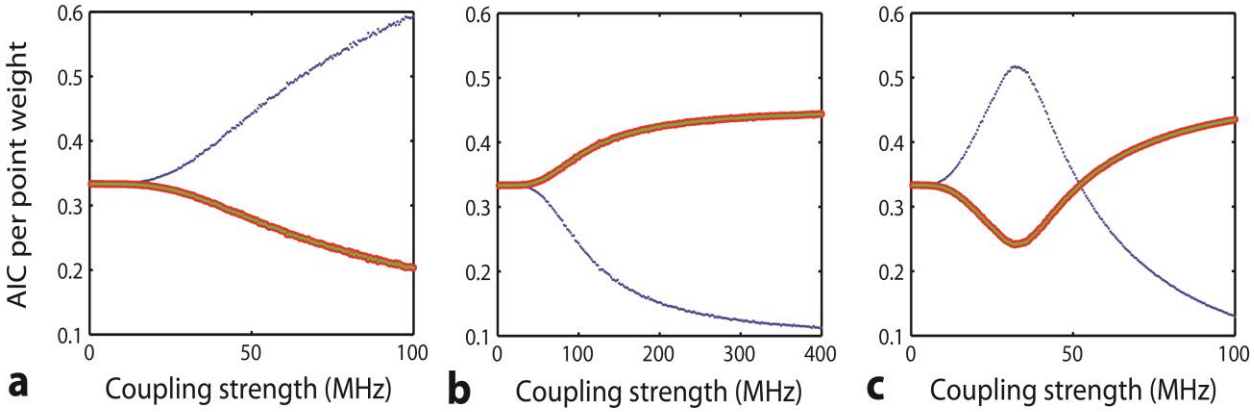

Supplementary Figure 4. Theoretical (noise model) AIC per-point weights as the function of coupling strength for EIT, ATS, and EIT/ATS (intermediate-driving models). *(Blue:* w_{EIT} *,green:* $w_{\mathrm{EIT/ATS}}$*, red and thicker:* w_{ATS}*)* ***(a)*** *The AIC per-point weight for the mode pair with* $Q\sim(1.91\times10^{5},7.26\times10^{7})$*.* ***(b)****The AIC per-point weight for the mode pair with* $Q\sim(1.63\times10^{6},1.54\times10^{6})$*.* ***(c)*** *The AIC per-point weight for the mode pair with* $Q\sim(1.78\times10^{6},4.67\times10^{6})$*. The values of the parameters used in* ***(a)-(c)*** *are typical parameters observed in our experiments. Pairs of quality factors are the ones measured in the experiments (see* ***Supplementary Fig. 5****).*

Supplementary Figure 5

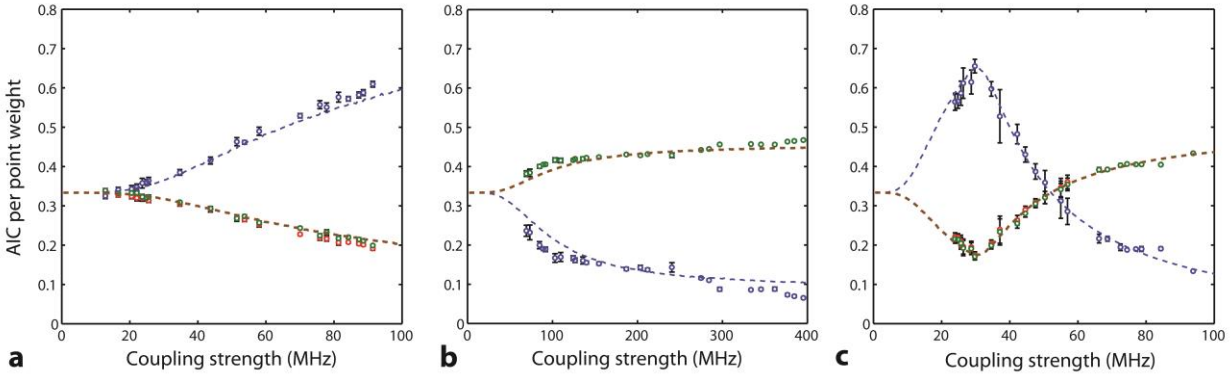

Supplementary Figure 5. Experimental AIC per-point weights as the function of coupling strength for EIT, ATS, and EIT/ATS (intermediate-driving models). *(Blue:* w_{EIT} *,green:* $w_{\mathrm{EIT/ATS}}$*, red and thicker:* w_{ATS}*)* ***(a)*** *The AIC per-point weight for the mode pair with* $Q\sim(1.91\times10^{5},7.26\times10^{7})$*.* ***(b)****The AIC per-point weight for the mode pair with* $Q\sim(1.63\times10^{6},1.54\times10^{6})$*.* ***(c)*** *The AIC per-point weight for the mode pair with* $Q\sim(1.78\times10^{6},4.67\times10^{6})$*.*

Supplementary Figure 6

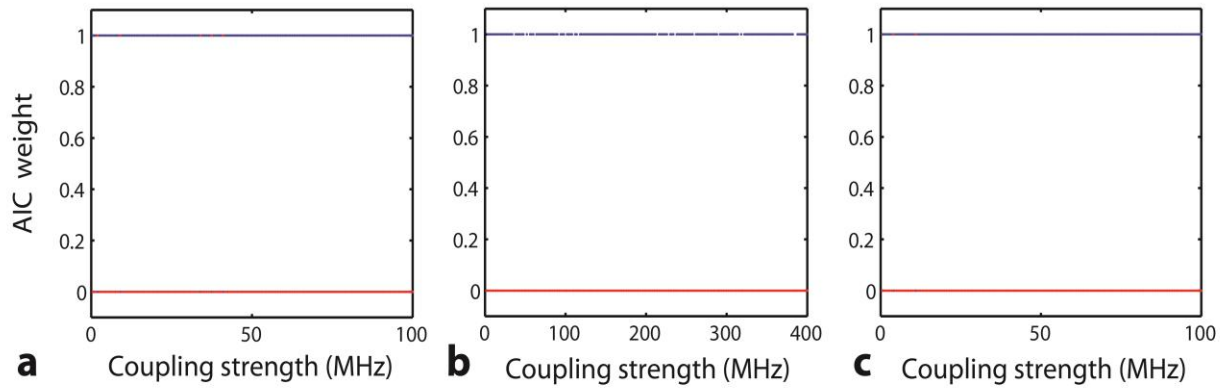

Supplementary Figure 6. Theoretical (noise model) AIC weights as the function of coupling strength for ATS and EIT/ATS models. *(Blue: w_{ATS}, red: $w_{\mathrm{EIT/ATS}}$) (**a**) The AIC per-point weight for the mode pair with $Q\sim(1.91\times10^{5},7.26\times10^{7})$. (**b**) The AIC per-point weight for the mode pair with $Q\sim(1.63\times10^{6},1.54\times10^{6})$. (**c**) The AIC per-point weight for the mode pair with $Q\sim(1.78\times10^{6},4.67\times10^{6})$.*

Supplementary Figure 7

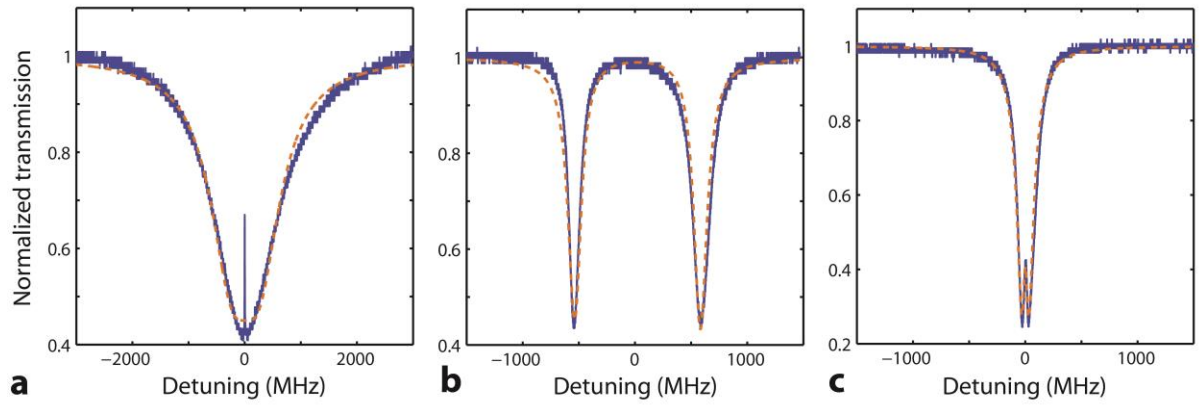

Supplementary Figure 7. Fitting with the intermediate-driving model to the experimentally obtained spectra. *Blue: experiment, Orange: Intermediate-driving model fitting.* ***(a)*** *The fitting spectra for the mode pair with* $Q\sim(1.91\times10^5, 7.26\times10^7)$. ***(b)*** *The AIC fitting spectra for the mode pair with* $Q\sim(1.63\times10^6, 1.54\times10^6)$. ***(c)*** *The fitting spectra for the mode pair with* $Q\sim(1.78\times10^6, 4.67\times10^6)$.

Supplementary Note 1:

Theoretical Model and Numerical Simulations

Here we give the results of numerical simulations depicting the expressions derived in the subsection *"Analogy between coupled optical resonators and three-level atoms"* of the main text for different driving regimes. As shown in the main text, for the coupled resonator system, the output field is given as $A_{\text{out}} = A_{\text{p}} + \sqrt{\gamma_{\text{c}}} A_1$ where the intracavity field A_1 can be written as $A_1 = i\sqrt{\gamma_{\text{c}}} A_{\text{p}} \chi$ with

$$\chi = \frac{(\omega + i\alpha_2)}{\kappa^2 - (\omega + i\alpha_1)(\omega + i\alpha_2)} \tag{1}$$

where we used $\alpha_k = i\omega_k + \gamma_k / 2$ with $k = 1, 2$. This solution χ has a form similar to the response of an EIT medium (three-level atom) to a probe field. The normalized transmission $T = \left| A_{\text{out}} / A_{\text{p}} \right|^2$ is written as

$$T = 1 + \gamma_{\text{c}}^2 \left| \chi \right|^2 - 2\gamma_{\text{c}} \chi_{\text{i}} . \tag{2}$$

with χ_{i} representing the imaginary part of χ. Since $1 >> \gamma_{\text{c}}^2 \left| \chi \right|^2$ and $\gamma_{\text{c}}^2 \left| \chi \right|^2 << \gamma_{\text{c}} \chi_{\text{i}}$ we can re-write the transmission as

$$T = 1 - 2\gamma_{\text{c}} \chi_{\text{i}} \tag{3}$$

Clearly, it will be sufficient to analyze the behavior of χ_{i} only to understand the conditions leading to EIT or ATS. This is similar to considering the imaginary part of the susceptibility which determines the absorption of a probe in an atomic system.

We can re-write the expression in Eq.(1) as

$$\chi = \frac{\chi_+}{\omega - \omega_+} + \frac{\chi_-}{\omega - \omega_-} \tag{4}$$

where $\omega_{\mp}$ are the eigenfrequencies of the coupled system, $\chi_{\pm} = \mp(\omega_{\pm} + i\alpha_2)/\beta = -1/2 \pm i\xi/\beta$ satisfying $\chi_+ + \chi_- = -1$ and $\xi = (\gamma_1 - \gamma_2)/4$. Depending on the system parameters, we have three different driving regimes[1,2,3,4]:

(a) Weak-driving regime ($\kappa < \kappa_T$). In this regime β is imaginary, that is $\beta = i\beta_i$ and $\mathrm{Re}(\beta) = \beta_r = 0$ leading to real $\chi_\pm$ (i.e., $\mathrm{Im}(\chi_\pm) = \chi_{\pm i} = 0$) with $\mathrm{Re}(\chi_\pm) = \chi_{\pm r} = -1/2 \pm \xi/|\beta|$, and imaginary eigenfrequencies (i.e., $\mathrm{Re}(\omega_\pm) = \omega_{\pm r} = 0$) with $\mathrm{Im}(\omega_\pm) = \omega_{\pm i} = -\zeta \pm |\beta|$ where $\zeta = (\gamma_1 + \gamma_2)/4$. Thus the supermodes have the same resonance frequencies and are located at the center of the frequency axis, but they have different linewidths quantified by their imaginary parts. As a result, the real and imaginary parts of χ become

$$\chi_r = \frac{\omega \chi_{+r}}{\omega^2 + \omega_{+i}^2} + \frac{\omega \chi_{-r}}{\omega^2 + \omega_{-i}^2} \tag{5}$$

$$\chi_i = \frac{\omega_{+i} \chi_{+r}}{\omega^2 + \omega_{+i}^2} + \frac{\omega_{-i} \chi_{-r}}{\omega^2 + \omega_{-i}^2} \tag{6}$$

from which we write the transmission as

$$T_{EIT} = 1 - 2\gamma_c \chi_i = 1 - 2\gamma_c \left[\frac{\omega_{+i} \chi_{+r}}{\omega^2 + \omega_{+i}^2} + \frac{\omega_{-i} \chi_{-r}}{\omega^2 + \omega_{-i}^2} \right] = 1 - \frac{C_1}{\omega^2 + \Gamma_1^2} + \frac{C_2}{\omega^2 + \Gamma_2^2}. \tag{7}$$

We have plotted the expressions in Eqs. (5)-(7) in **Supplementary Fig. 1** which shows that the normalized transmission becomes maximum around the zero frequency-detuning exactly where the imaginary part of χ becomes minimum. Clearly the transmission behavior of the system is determined by the χ_i .

(b) Strong-driving regime ($\kappa >> \kappa_T$). In this regime $\beta = 2\kappa$ is real (i.e., $\beta_i = 0$ and $\beta_r = 2\kappa$) implying $\omega_\pm = -i\zeta \pm \kappa$, that is the resonances are located at frequencies $\pm\kappa$ with a spectral distance of 2κ between them. The linewidths of the resonances are quantified by $\mathrm{Im}(\omega\pm) = -\zeta/4$. Moreover, we can approximate $\chi_\pm$ as $\chi_\pm = -1/2$. Then we can write the imaginary parts of χ as

$$\chi_r = -\frac{1}{2} \left[\frac{\omega - \kappa}{(\omega - \kappa)^2 + \zeta^2} + \frac{\omega + \kappa}{(\omega + \kappa)^2 + \zeta^2} \right] \tag{8}$$

$$\chi_{\mathrm{i}} = \frac{1}{2}\left[\frac{\zeta}{(\omega-\kappa)^2+\zeta^2} + \frac{\zeta}{(\omega+\kappa)^2+\zeta^2}\right] \tag{9}$$

Consequently, the transmission in this regime becomes

$$T_{\mathrm{ATS}} = 1-\gamma_{\mathrm{c}}\left[\frac{\zeta}{(\omega-\kappa)^2+\zeta^2} + \frac{\zeta}{(\omega+\kappa)^2+\zeta^2}\right] = 1-\frac{C}{(\omega-\delta_0)^2+\Gamma^2} - \frac{C}{(\omega-\delta_0)^2+\Gamma^2} \tag{10}$$

with $\delta_0 \approx \pm\kappa$. We have plotted T_{ATS} using the parameters obtained in the experiments and depicted it in **Supplementary Fig. 2**. Clearly, imaginary part of the susceptibility function determines the normalized transmission which consists of two Lorentzian resonances separated by 2κ. We should note that χ_i shows Lorentzian peaks whereas the normalized transmission shows Lorentzian dips with a larger transparency window than that of the transmission spectra obtained for the weak-driving regime (EIT case).

(c) Intermediate-driving regime ($\kappa > \kappa_{\mathrm{T}}$). In this regime $\beta = \beta_{\mathrm{r}}$ is real (i.e., $\beta_{\mathrm{i}} = 0$). This leads to complex eigenfrequencies $\omega_{\pm} = \left(-i\gamma_1 - i\gamma_2 \pm 2\beta_{\mathrm{r}}\right)/4$ (i.e., $\mathrm{Re}\left(\omega_{\pm}\right) = \omega_{\pm r} \neq 0$ and complex $\chi_{\pm}$ (i.e., $\mathrm{Im}\left(\chi_{\pm}\right) = \chi_{\pm\mathrm{i}} \neq 0$). Then $\mathrm{Im}\left(\chi_{\pm}\right) = \chi_{\pm\mathrm{i}} = \pm\left(\gamma_1-\gamma_2\right)/4|\beta|$ with $\mathrm{Re}\left(\chi_{\pm}\right) = \chi_{\pm\mathrm{r}} = -1/2$. The real and imaginary parts of the eigenfrequencies are $\mathrm{Re}\left(\omega_{\pm}\right) = \omega_{\pm\mathrm{r}} = \pm\beta/2$ and $\mathrm{Im}\left(\omega_{\pm}\right) = \omega_{\pm\mathrm{i}} = \left(-\gamma_1-\gamma_2\right)/4$, respectively. Thus the supermodes have different resonance frequencies which are located at $\pm\beta/2$, but have the same linewidths quantified by their imaginary parts $\mathrm{Im}\left(\omega_{\pm}\right) = \omega_{\pm\mathrm{i}} = \left(-\gamma_1-\gamma_2\right)/4$. Consequently, we the real and imaginary parts of χ become

$$\chi_{\mathrm{r}} = \frac{(\omega-\omega_{+\mathrm{r}})\chi_{+\mathrm{r}} - \omega_{+\mathrm{i}}\chi_{+\mathrm{i}}}{(\omega-\omega_{+\mathrm{r}})^2+\omega_{+\mathrm{i}}^2} + \frac{(\omega-\omega_{-\mathrm{r}})\chi_{-\mathrm{r}} - \omega_{-\mathrm{i}}\chi_{-\mathrm{i}}}{(\omega-\omega_{-\mathrm{r}})^2+\omega_{-\mathrm{i}}^2} \tag{11}$$

$$\chi_{\mathrm{i}} = \frac{(\omega-\omega_{+\mathrm{r}})\chi_{+\mathrm{i}} + \omega_{+\mathrm{i}}\chi_{+\mathrm{r}}}{(\omega-\omega_{+\mathrm{r}})^2+\omega_{+\mathrm{i}}^2} + \frac{(\omega-\omega_{-\mathrm{r}})\chi_{-\mathrm{i}} + \omega_{-\mathrm{i}}\chi_{-\mathrm{r}}}{(\omega-\omega_{-\mathrm{r}})^2+\omega_{-\mathrm{i}}^2} \tag{12}$$

which imply that χ_i is the sum of two same-sign quasi-Lorentzians centered at $\pm\beta/2$. The transmission at this region is then given as

$$T_{\mathrm{EIT/ATS}} = 1 - 2\gamma_{\mathrm{c}}\chi_{\mathrm{i}} = 1 - 2\gamma_{\mathrm{c}}\left[\frac{(\omega-\omega_{+\mathrm{r}})\chi_{+\mathrm{i}} + \omega_{+\mathrm{i}}\chi_{+\mathrm{r}}}{(\omega-\omega_{+\mathrm{r}})^2+\omega_{+\mathrm{i}}^2} + \frac{(\omega-\omega_{-\mathrm{r}})\chi_{-\mathrm{i}} + \omega_{-\mathrm{i}}\chi_{-\mathrm{r}}}{(\omega-\omega_{-\mathrm{r}})^2+\omega_{-\mathrm{i}}^2}\right]$$

$$= 1 - 2\gamma_{\mathrm{c}}\left\{\left[\frac{(\omega-\omega_{+\mathrm{r}})\chi_{+\mathrm{i}}}{(\omega-\omega_{+\mathrm{r}})^2+\omega_{+\mathrm{i}}^2} + \frac{(\omega-\omega_{-\mathrm{r}})\chi_{-\mathrm{i}}}{(\omega-\omega_{-\mathrm{r}})^2+\omega_{-\mathrm{i}}^2}\right] + \left[\frac{\omega_{+\mathrm{i}}\chi_{+\mathrm{r}}}{(\omega-\omega_{+\mathrm{r}})^2+\omega_{+\mathrm{i}}^2} + \frac{\omega_{-\mathrm{i}}\chi_{-\mathrm{r}}}{(\omega-\omega_{-\mathrm{r}})^2+\omega_{-\mathrm{i}}^2}\right]\right\} \quad (13)$$

$$= 1 - \left\{\left[\frac{(\omega-\varepsilon)C_1}{(\omega-\varepsilon)^2+\Gamma^2} - \frac{(\omega+\varepsilon)C_1}{(\omega+\varepsilon)^2+\Gamma^2}\right] + \left[\frac{C_2}{(\omega-\varepsilon)^2+\Gamma^2} + \frac{C_2}{(\omega+\varepsilon)^2+\Gamma^2}\right]\right\}$$

where the second expression in the bracket is similar to the expression derived for the strong-driving regime (ATS case). Thus we re-write Eq. (13) as

$$T_{\mathrm{EIT/ATS}} = T_{\mathrm{ATS}} - C_1\left[\frac{(\omega-\varepsilon)}{(\omega-\varepsilon)^2+\Gamma^2} - \frac{(\omega+\varepsilon)}{(\omega+\varepsilon)^2+\Gamma^2}\right] \quad (14)$$

Supplementary Fig. 3 depicts the transmission function given in Eq. 14 together with the real and imaginary parts of the susceptibility.

Supplementary Note 2:

Comparison among weak-driving regime (EIT), strong driving regime (ATS), and Intermediate-driving (EIT/ATS) models using the Akaike Information Criterion.

In the main text, although we have derived the normalized transmission for weak, strong and intermediate driving regimes, in the model selection problem we used only the expressions for EIT (weak driving regime) and ATS (strong driving regime). The reason behind this was that the model for the intermediate-driving regime EIT/ATS contains two terms2: One is exactly the same as the expression derived for the strong driving regime (ATS) and the other is an interference term whose contribution can be set to zero or minimized by properly choosing the coupled modes or is set to zero or much lower values than the contribution from the ATS part during the curve-fitting algorithm due to the fact that C_1 is a free-parameter. Here we give the results of our study in which we performed curve fitting using the EIT, ATS and EIT/ATS models to the calculated theoretical transmission spectra obtained using experimentally relevant parameter values. In the transmission spectra we also included 1% Gaussian noise. Moreover, we give the AIC per-point weights for the three driving regimes.

We have observed that the ATS and the EIT/ATS models have the same AIC per-point weights5. Results obtained for typical transmission spectra are depicted in **Supplementary Fig. 4**. As the coupling strength increases, the $\bar{w}_{\mathrm{ATS}}$ and $\bar{w}_{\mathrm{EIT/ATS}}$ exhibit the same values. This is expected as we have mentioned above that the transmission in the intermediate-driving regime includes the contribution from the ATS model as shown in Eq. (14). Therefore, the $\bar{w}_{\mathrm{ATS}}$ and $\bar{w}_{\mathrm{EIT/ATS}}$ are always have similar values as the system evolves from weak to strong driving regimes. These agree well with our experimental observations depicted in **Supplementary Fig. 5**.

We also checked the difference between the ATS (strong driving regime) and the EIT/ATS (intermediate driving regime) models by calculating the AIC weights5 without the averaging effect. The binary weights in **Supplementary Fig. 6** reveals that the AIC weights of the EIT/ATS model is always lower than those of ATS model, because although the EIT/ATS model gives a more precise fitting to the experimental data, the higher number of free parameters in the EIT/ATS model adds larger cost (i.e., increased penalty) and hence reduces the weights of this model.

Finally, we used the intermediate driving model (EIT/ATS) to fit to the typical transmission spectra obtained in our experiments. The results are depicted in **Supplementary Fig. 7**. It is seen that for the transmission spectra for EIT case (same as the one in the main text), the EIT/ATS model do not provide a good fit although it has more free parameters. The discrepancy is significant around the zero-detuning where we have the transparency window. For the spectra obtained for the ATS and EIT-to-ATS transition, we see that the EIT/ATS model provides a curve-fitting at least as good as the ATS model.

Supplementary References.

1. Sun H., Liu Y.X., You, J.Q., Il'ichev E., Nori F. Electromagnetically induced transparency and Autler-Townes splitting in superconducting flux quantum circuits. *arXiv:1310.7323* (2013).
2. Tan, C., and Huang, G. Crossover from electromagnetically induced transparency to Autler–Townes splitting in open ladder systems with Doppler broadening. JOSA B, 31, 704-715 (2014).
3. Abi-Salloum, T.Y. Electromagnetically induced transparency and Autler-Townes splitting: Two similar but distinct phenomena in two categories of three-level atomic systems. *Phys. Rev. A.* **81**, 053836 (2010).
4. Abi-Salloum, T.Y., Davis, J.P., Lehman, C., Elliott, E., and Narducci, F.A. Phase dynamics and interference in EIT. *J. Mod. Opt.* 54, 2459-2471 (2007).
5. Anisimov, P. M., Dowling, J. P., and Sanders, B. C. Objectively discerning Autler-Townes splitting from electromagnetically induced transparency. *Phys. Rev. Lett.* **107**, 163604 (2011).